Numerical Investigations of Aerodynamics Performance of Blunt Nose Cone with Aerodisk at Hypersonic Flow

Jhanvi Chauhan, G. Balaji, Monika Swastikar, G. Boopathy, S. Sangeetha, G. Santhosh Kumar, and G. M. Pradeep

Abstract

The blunted nose cone with and without a sharp aerospike and an aerodisk of various diameters and lengths are investigated numerically in detail in the current study at a hypersonic Mach number of 10. The aerodisk diameter is described as d/D ratios such as 0.2, 0.4 and 0.6, and the length of the aerospike is represented as the L/D ratio of 1, 1.5 and 2. The main objective of the research is to examine the aerodynamic properties of blunt noses with and without aerodisks and aerospikes, as well as the influence of shock production over the model. The design of blunted nose cones with aerodisk was made up using CATIA and numerical investigation was performed on the ANSYS Fluent. The turbulence model of SST k-omega was considered for study. The current study revealed that shock patterns drastically varied nearer to the nose cone model at L/D ratio 2 and variation of drag reduction occurred due to the increase in d/D ratio and aerospike and also flow pattern over the model was clearly investigated.

Keywords

Aerodisk • Spike • ANSYS fluent • CFD • Blunt nose cone

1 Introduction

High speed vehicles that travel at hypersonic speeds such as spacecraft, launch vehicles, missiles, and re-entry vehicles, typically use a blunt nose body to reduce the heat. In hypersonic vehicles, as Mach numbers get larger, factors like viscous interactions, very high temperatures, formation of a thin shock layer and entropy layer became the highest priority. Excessive aerodynamic drag and aerodynamic heating transmit major obstacles for hypersonic vehicles. At supersonic and hypersonic speeds, the flow over a blunt body generates a bow shock wave that leads to massive surface pressure and severe aerodynamic drag. When in atmospheric flight, blunt bodies with high Mach numbers create a bow shock wave which raises the wave drag significantly and causes heating in the aerodynamic region by exerting a tremendous amount of pressure on the forward-facing area of the body. By creating an area of consistent low pressure in front of the body, which is dull and blunt, the dynamic pressure is reduced. Therefore, in order to reduce the aerodynamic drag and aerodynamic heating, the aerodisk attached with a spike is used which is a simple and useful method.

As bow shock plays an important role for hypersonic vehicles due to the blunt nose shape causing resistance for that reason aerodisk in the frontal area, so that bow shock converts into weak oblique shock. This oblique shock can be penetrated easily with a balance of every parameter. Now oblique shock coming near the body causes high heating issues which can be a high risk of damage to the vehicle. Aerodisk along with an appropriate length of aerospike attachment is there for heat dissipation around the atmosphere.

J. Chauhan · G. Balaji (✉) · M. Swastikar · S. Sangeetha
Department of Aeronautical Engineering, Hindustan Institute of Technology and Science, Padur, Chennai, 603103, India
e-mail: gbalajihits@gmail.com

G. Boopathy
Department of Aeronautical Engineering, Vel Tech Rangarajan Dr. Sagunthala R&D Institute of Technology and Science, Chennai, 600062, India

G. Santhosh Kumar
Department of Mechanical Engineering, University College of Engineering, Bharathidasan Institute of Technology Campus, Anna University, Tiruchirappalli, Tamil Nadu, India

G. M. Pradeep
Department of Mechatronics Engineering, Vellammal Institute of Technology, Chennai, Tamil Nadu, India

M. Sumesh et al. (eds.), *2nd International Conference on Smart Sustainable Materials and Technologies (ICSSMT 2023)*, Advances in Science, Technology & Innovation, https://doi.org/10.1007/978-3-031-50024-4_18

Schnepf et al. (2015) simulated the wave drag reduction of the blunt slender body with the help of a self-alignment aerodisk and the complete missile configuration was qualitatively studied. Further observed that AD performance was interesting at much greater repetition rates and Mach numbers with available experimental data and taking into account the aerodisk's kinematics and structure when being shocked and separated, there is qualitatively good agreement. The distinct reduction of drag was achieved in comparison with the reference body without a self-alignment aerodisk. Wysocki et al. (2014) conducted the experimental study of wave drag reduction using self-aligning aerospike on slender body and research done in the transonic wind tunnel under dynamic as well as static environments. Self-aligning aerospikes have been found to reduce blunt-nosed slender bodies' overall drag by up to 25–30% for Mach numbers, which are present in the range of M = 1.4 and M = 2.2 and it is observed that it helps to fast pitching maneuver in the flow directions.

Deng et al. (2017) numerically investigated the spike effect on drag reduction for hypersonic lifting bodies. To find the optimal disc for reducing hypersonic drag, three alternative aerospike disc designs are studied. The twin flat-faced disc aerospike offers the best drag reduction, reducing pressure drag by 60.5% of the nose's portion at an angle of 8 degrees. Additionally, there is a large increase in drag as the flying angle of attack increases. The 1.6% advance in the pressure centre minimally affects the vehicle's vertical static stability. Hamid et al. (2022) worked on the two distinct geometries, such as two spherically blunted tangent aerodisks and two hemisphere aerodisks. These two geometries are simulated in OpenFOAM software. Understanding shock behaviour, aerodynamic drag, and thermal loading was the main objective of this study. The nose cone attached to the aerodisk has drag that is only 12% of the baseline case of the blunt nose cone, demonstrating that the effectiveness of the two-tangent gives aerodisks with spherically blunted ends in lowering drag. The separation region which is created by the aerodisk is the primary reason for the drag reduction.

Elsamanoudy et al.'s (2013) After Reattachment Ring for Hypersonic Hemispherical Bodies and Drag Reduction Using Spiked-Aerodisks was studied, it is demonstrated that the reattachment ring, which is positioned exactly on the reattachment point, can be used to lessen the high pressure and aerodynamic heating created there. The simulation was performed using ANSYS Fluent. The reattachment ring, with dimensions of 0.1D in height and 0.025D in thickness, was a concept that the authors introduced. The ring's reattachment points experience the highest pressure and heating. It utilizes an unstructured mesh. The various models underwent rigorous testing at high Reynolds numbers Re of 4, 5, and 6, 106, as well as high Mach numbers 6, 8, and 10. At a height of 25 km, the models are evaluated. Senthilkumar et al. (2021) A forward-facing spike was fixed to a hemispherical body generating a recirculation area that circles the area of stagnation of the dull and blunt body, significantly transforms the structure of the flow field and lowers the drag. Because of the geometry of the back-disk, the flow field immediately behind the Aerodisks is more complicated than the flow field directly in front of the conical spike. In order to understand and make most of the spike that is facing forward for more efficient drag reduction, the area of the reattachment point in the shear layer present on the body has to be moved in the backward region by choosing the spike that is similar to the perfect length with the proper arrangement of geometrical part of the nose.

Balaji et al. (2015) the improvement of Blunt Body's Aerodynamic Performance using Aero Disc, the author worked on the hemisphere aerodisk attached with a spike with different diameters of the aerodisk. They used different diameters like 0.1D, 0.15D and 0.2D, where D is blunt nose diameter. Overall spike to aerodisk length L/D ratio is 1. The spike effects on the Hypersonic lifting body have been examined for aerodynamics properties such as drag reduction, by numerical analysis and comparing the lifting body at 40 km altitude and Mach 8 when equipped with and without an Aerodisk. A numerical simulation of the flow over the vehicle with hemispheric disc aerospikes at various length-to-diameter ratios is performed. For an L/D ratio of 2.0, the hemispheric aerodisk aerospike and a flat conical aerodisk aerospike are compared in order to know about the flow field characteristics and techniques which are related to the reduction of drag. Effect of blunted aerodisk on the blunt nose that is actually aero-spiked cone at a superior velocity**,** they worked on the blunt nose cone, aerospike with different L/D ratios, hemispherical aerodisk and blunted aero disk. Kalimuthu et al. (2008) did some experimental research, and it was discovered that the Aerodisk is having more superiority and versatility in comparison to the aerospike. Additionally, it has been found that an Aerodisk with the right length, diameter, and nose configuration can lessen the drag on hypersonic vehicles (Balaji et al., 2022). The attachment of an aerodisk after fixing to the leading edge of the spike will help in the drag reduction mechanism. Thought must be given to the increased moment caused by the spike if it is at an angle of attack.

In the current research work, the consequences of aerospike and aerodisk over the blunted nose are investigated for a different hypersonic Mach number 10. The diameter of the hemispherical aerodisk changes for different d/D ratios such as 0.2, 0.3 and 0.4, where d is the diameter of the aerodisk, and D is the blunt body diameter. The aerodisk is positioned at different locations of the location of aerospike length described as an L/D ratio of 1,1. 5 and 2, where L is the length of aerospike. The blunt body's diameter serves as the

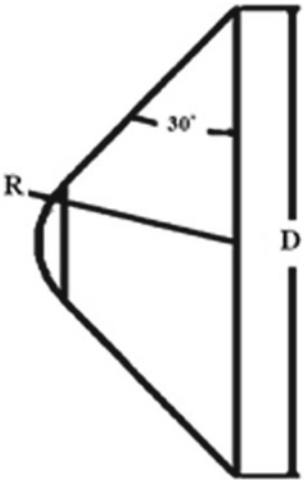

Fig. 1 Schematic diagram of blunt nose cone

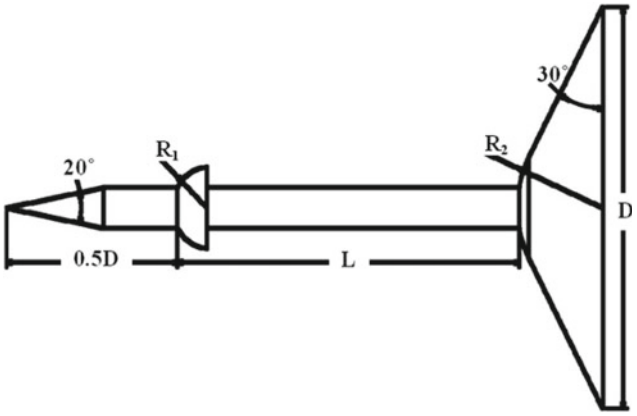

Fig. 2 Schematic diagram of blunt nose cone with aerospike and aerodisk

foundation for the entire structure. The terms "blunted nose" and "blunted nose with aerospike and aerodisk placed in front of the nose cone" refer to two distinct nose cone configurations. The drag coefficients and lift coefficients are measured for different geometries of the nose cone model. This study demonstrates the influence of shock waves from the blunted nose and spiked contacts with aerodisk cones to understand the source of drag reduction and geometry as shown in Figs. 1 and 2.

2 CFD Methodology

In this research work, ANSYS Workbench is used to produce unstructured grids over the blunted nose and the blunted nose with aerospike and aerodisk. The entire surface of the nose cone is generated with an unstructured grid for both cases as shown in Figs. 3 and 4. The flow around the blunt nose cone body is attached to aerodisk which is analysed by ANSYS Fluent. The computation of the flow field incorporates boundary conditions, such as the velocity inlet, velocity outlet, wall, and pressure far field conditions. The simulation of the blunt nose is carried out for various Mach numbers of 10.

The model of a hemispherical aerodisk is attached with a sharp spike and blunt body is designed in ANSYS Design Modeler. A CFD domain was created around the body and The CFD domain was given a name like inlet, outlet, symmetry, wall, and pressure far field. The meshing is generated over the model with an unstructured grid with a count of 150,000 cells. The Gauge pressure, Temperature and operating conditions are 26,425 Pa, 233 K and 0 Pa, respectively. For analysis of the CFD domain, the flow is considered as compressible, density-based solver used and also Turbulence model is considered as the SST k-omega model. The governing equations used for the turbulence model are described. The Shear Stress Transport k-omega model's transport equation variables are comparable to

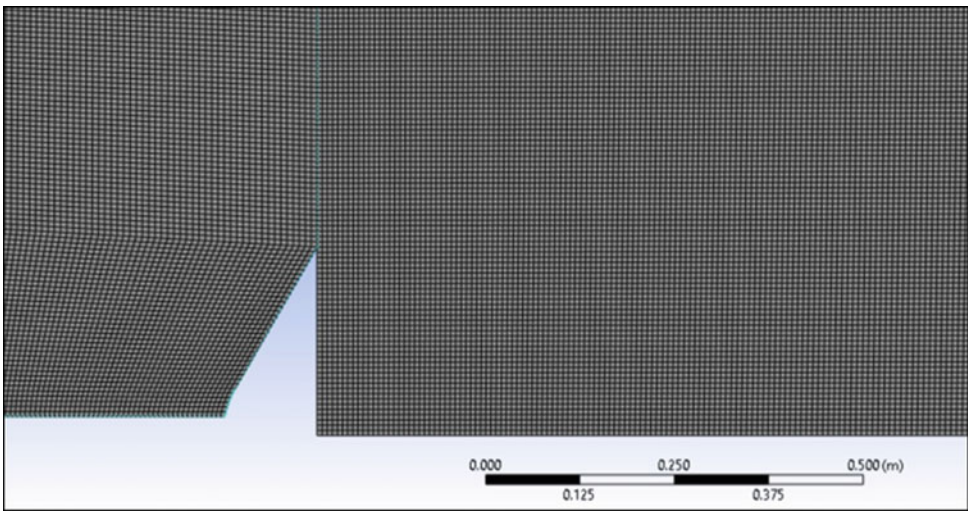

Fig. 3 Meshing of the blunt nose cone

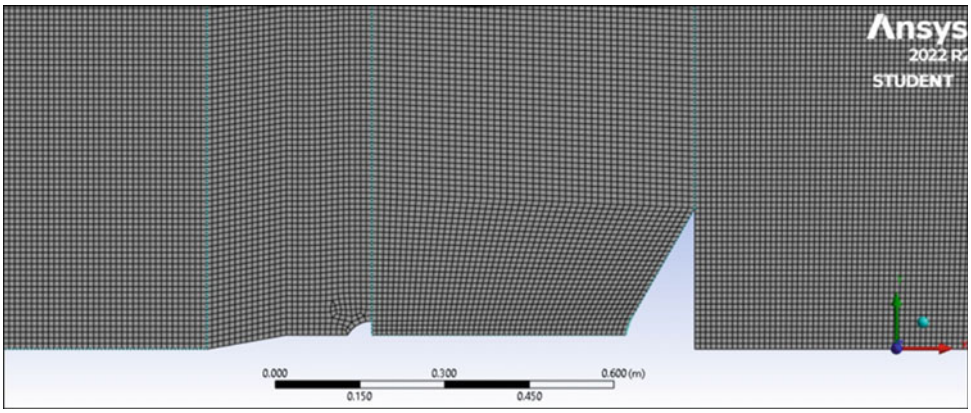

Fig. 4 Meshing of blunt nose cone with aerodisk and aerospike

turbulence's kinematic viscosity, with the exception of the viscous-affected region close to the wall. The transport equation related to the kinematic viscosity (v) is given by

$$\frac{\partial}{\partial t}(\rho v) + \frac{\partial}{\partial x_i}(\rho v x_i) = G_v + \frac{1}{\sigma_v}\left\{\frac{\partial}{\partial x_i}\left[(\mu + \rho v)\frac{\partial v}{\partial x_j}\right] + C_{b2}\rho\left(\frac{\partial v}{\partial x_i}\right)^2\right\} - Y_v + Sv \quad (1)$$

where

G_v is the generations of the turbulence viscosity, and σ_v and C_{b2} are the constants, due to viscous damping and wall blocking, Y_v is the degradation of the viscosity that is related to the eddy currents which is in close proximity to the wall zone. The viscosity of the molecular kinematics is. S is the user-defined source term represented in the Eq. (1).

3 Result and Discussion

Understanding the forebody's reattachment point requires knowledge of the shock contour plot. Understanding the amount of reattachment delay for varied aerodisk diameters and aerospike lengths is the goal of this study. The increase in aero disc diameter from the pressure coefficient plot is observed to cause a delay in shock reattachment on the forebody. Additionally, it has been discovered that shock reattachment has an impact on the forebody's pressure coefficient owing to the aerospike's diameter and aerospike length, and that the aero disk's diameter increases resulting in a reduction in drag. On reattachment, the importance of such an aerodisk structure is implied. Additional combinations are also being included in this research.

3.1 Pressure of Contour of Blunt Nose Cone with and Without Aerospike and Aerodisk at Different Mach Numbers

This paper looked at different instances of disc spike performance in the region of the hypersonic lifting body aerodynamics. The computer simulation of flow which is hypersonic over a spiky lifting body at a Mach number of 10 with various L/D ratios and d/D ratio of the blunt nose conoid which is hovering at angles of attack 0 at various L/D ratios and d/D ratios. The pressure distribution over the blunt cone was examined for a Mach number of 10, represented with pressure contour, velocity contour, and velocity vector plots, giving insight into flow physics to analyze the behavior to find the drag reduction and shock pattern over the blunt nose cone with and without L/D ratio and d/D ratio shown in Figs. 5, 6, 7, 8, 9, 10, 11, 12 and 13.

3.1.1 Pressure Contour at Different D/D Ratios, L/D = 1 and Mach Number, M = 10

By analyzing the flow evolution which was found in a close diameter circling the area of blunt nose cone with and without the aerodisk and also the aerospikes depicted in Fig. 5a–d explains this discrepancy. In Fig. 5a, the pressure contour is somewhat elevated upstream of the blunt nose cone and creates the shock pattern distant from the blunt

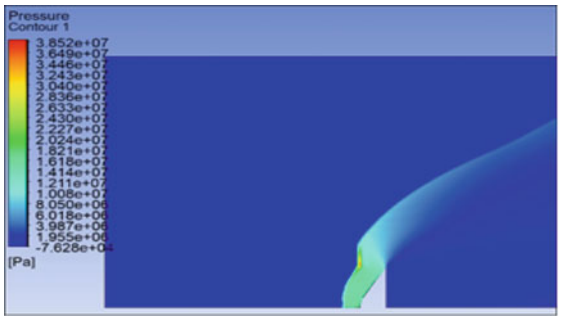

a. Pressure Contour on Blunt Nose Cone at M=10

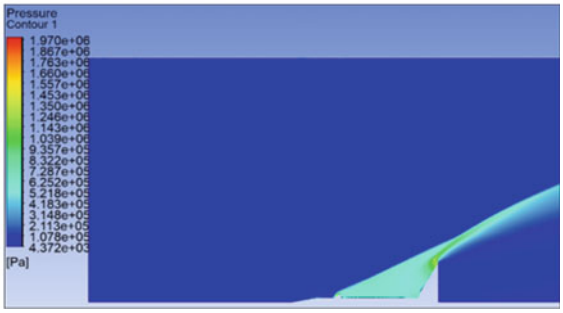

b. Pressure Contour on d/D = 0.2, L/D =1 & M = 10

c. Pressure Contour on d/D = 0.3, L/D =1 & M=10

d. Pressure Contour on d/D = 0.4, L/D =1, M=10

Fig. 5 Pressure distribution over the nose cone with and without aerospike and aerodisk at L/D ratio = 1

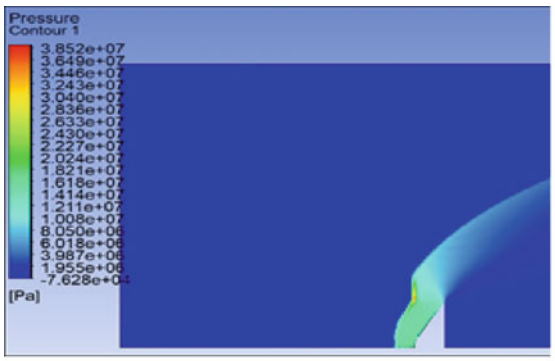

a. Pressure Contour on Blunt Nose Cone

b. Pressure Contour on d/D = 0.2, L/D =1.5 & M = 10

c. Pressure Contour on d/D = 0.3, L/D =1.5 & M = 10

d. Pressure Contour on d/D = 0.4, L/D =1.5 & M = 10

Fig. 6 Pressure distribution over the nose cone with and without aerospike and aerodisk at L/D ratio = 1.5

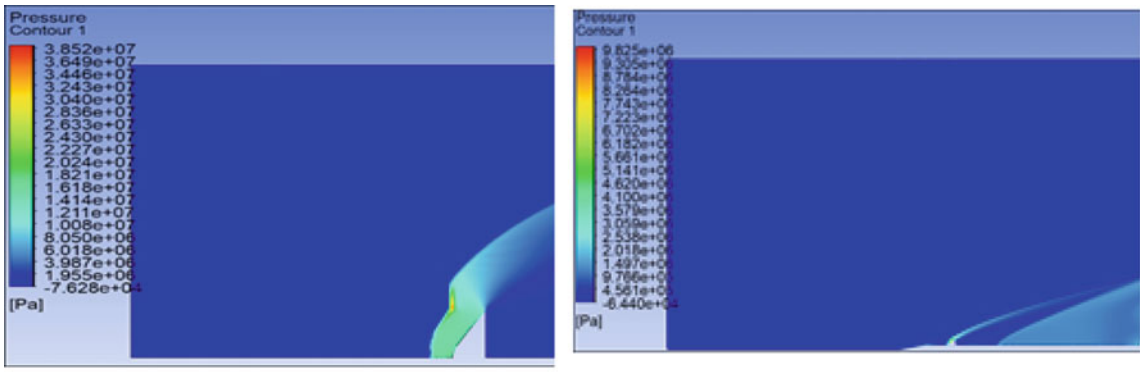

a. Pressure Contour on Blunt Nose Cone

b. Pressure Contour on d/D = 0.2, L/D = 2 & M = 10

c. Pressure Contour on d/D = 0.3, L/D = 2 & M =10

d. Pressure Contour on d/D = 0.4, L/D = 2 & M = 10

Fig. 7 Pressure distribution over the nose cone with and without aerospike and aerodisk at L/D ratio = 2

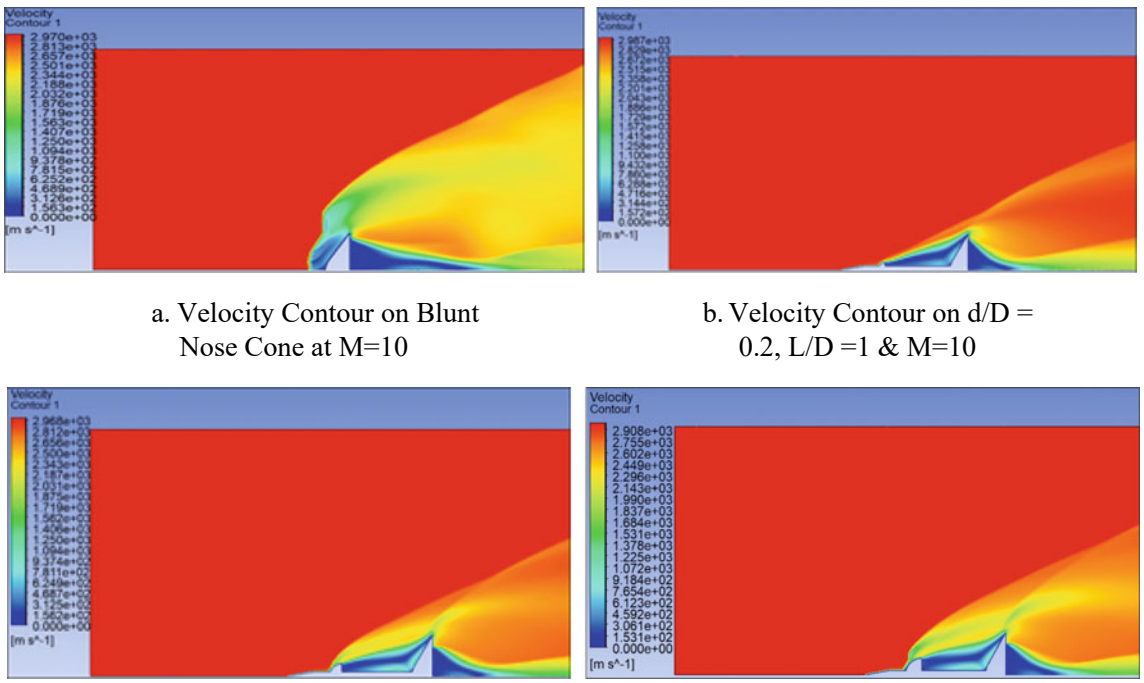

a. Velocity Contour on Blunt Nose Cone at M=10

b. Velocity Contour on d/D = 0.2, L/D =1 & M=10

c. Velocity Contour on d/D = 0.3, L/D 1 & M10

d. Velocity Contour on d/D = 04 L/D 1 M10

Fig. 8 Velocity distribution over the nose cone with and without aerospike and aerodisk at L/D ratio = 1

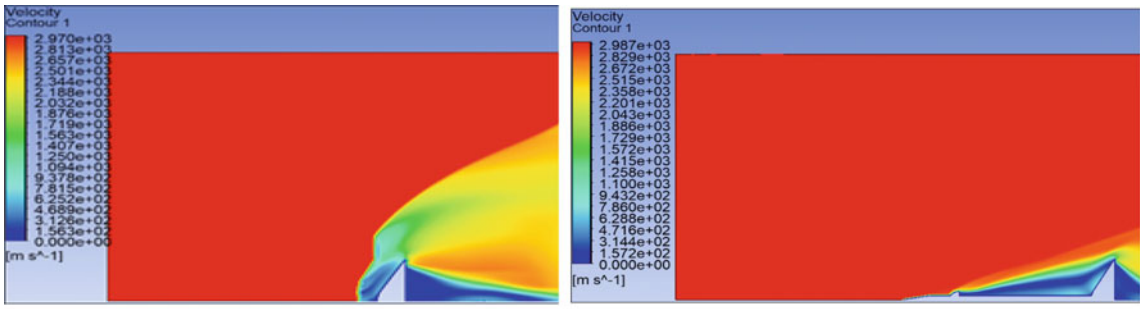

a. Velocity Contour on Blunt Nose Cone at M=10

b. Velocity Contour on d/D = 0.2, L/D =1.5 & M=10

c. Velocity Contour on d/D = 0.3 & L/D =1.5 & M=10

d. Velocity Contour on d/D = 0.4 & L/D =1.5 & M=10

Fig. 9 Velocity distribution over the nose cone with and without aerospike and aerodisk at L/D ratio = 1.5

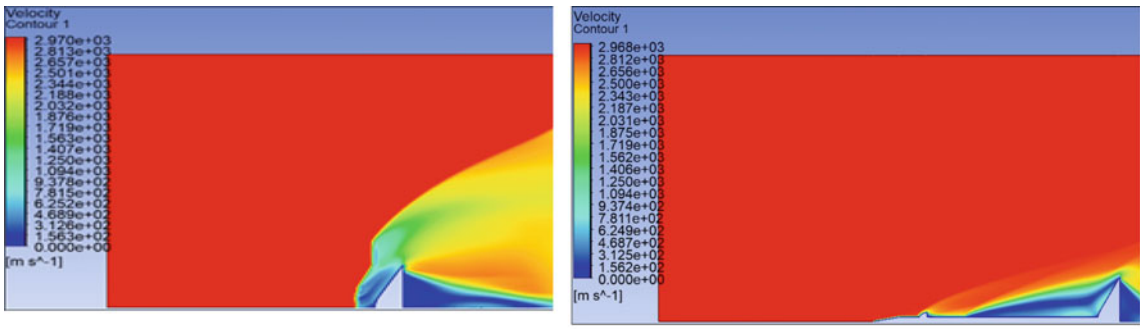

a. Velocity Contour on Blunt Nose Cone at M=10

b. Velocity Contour on d/D = 0.2, L/D = 2 & M=10

c. Velocity Contour on d/D = 0.3 & L/D = 2 & M=10

d. Velocity Contour on d/D = 0.4 & L/D = 2 & M=10

Fig. 10 Velocity distribution over the nose cone with and without aerospike and aerodisk at L/D ratio = 2

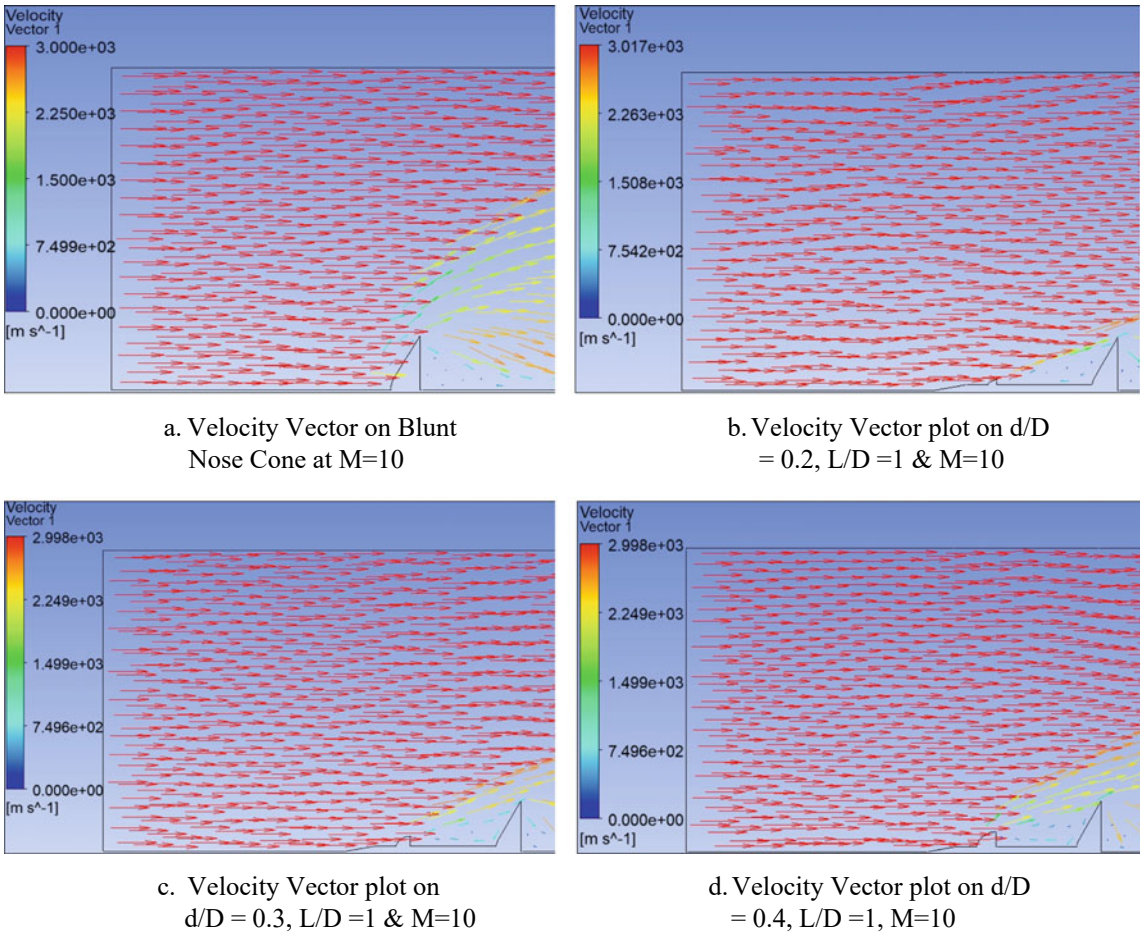

a. Velocity Vector on Blunt Nose Cone at M=10

b. Velocity Vector plot on d/D = 0.2, L/D =1 & M=10

c. Velocity Vector plot on d/D = 0.3, L/D =1 & M=10

d. Velocity Vector plot on d/D = 0.4, L/D =1, M=10

Fig. 11 Velocity Vector distribution over the nose cone with and without aerospike and aerodisk at L/D ratio = 1

nose cone's tip. The shock pattern that came into existence in the area of the nose cone that is blunted with aerodisk as well as aerospike has been demonstrated in Fig. 5b–d and the shock pattern intersects behind the nose cone. The strong shock pattern formation occurs at a d/D ratio of 0.2, 0.3 and 0.4 at the location of L/D = 1.

3.1.2 Pressure Contour at Different D/D, L/D = 1.5 and Mach Number, M = 10

Analysis and comprehension were done to find out why there is a difference, the flow file evolution of the dull nose canoed with the usage and also without the application of the aerodisk and aerospike shown in Fig. 6a–d is investigated. In Fig. 6a, the shock pattern is formed far from the blunt nose cone's tip by the pressure contour, which is slightly higher upstream of the blunt nose cone. Figure 6b–d depicts the shock pattern generation in the aerodisk and aerospike-equipped blunt nose cone as well as the intersecting shock pattern that forms behind the nose cone. The powerful shock pattern develops for d/D ratios of 0.2, 0.3, and 0.4 when L/D is equal to 1.5.

3.1.3 Pressure Contour at Different D/D, L/D = 2 and Mach Number, M = 10

To analyze and for an understanding of the differences, the evolution of the flow field around the blunt nose cone with and without the aerodisk and aerospike depicted in Fig. 7a–d is compared. The shock pattern is formed away from the blunt nose cone's tip by a minor increase in the pressure contour at Fig. 7a upstream of the cone's blunt tip. The shock pattern is formed in the blunt nose cone with an aerodisk and aerospike, as shown in Fig. 7b–d, and intersects with the shock pattern behind the nose cone very far away. At the ratio of L/D = 2, the creation of a very

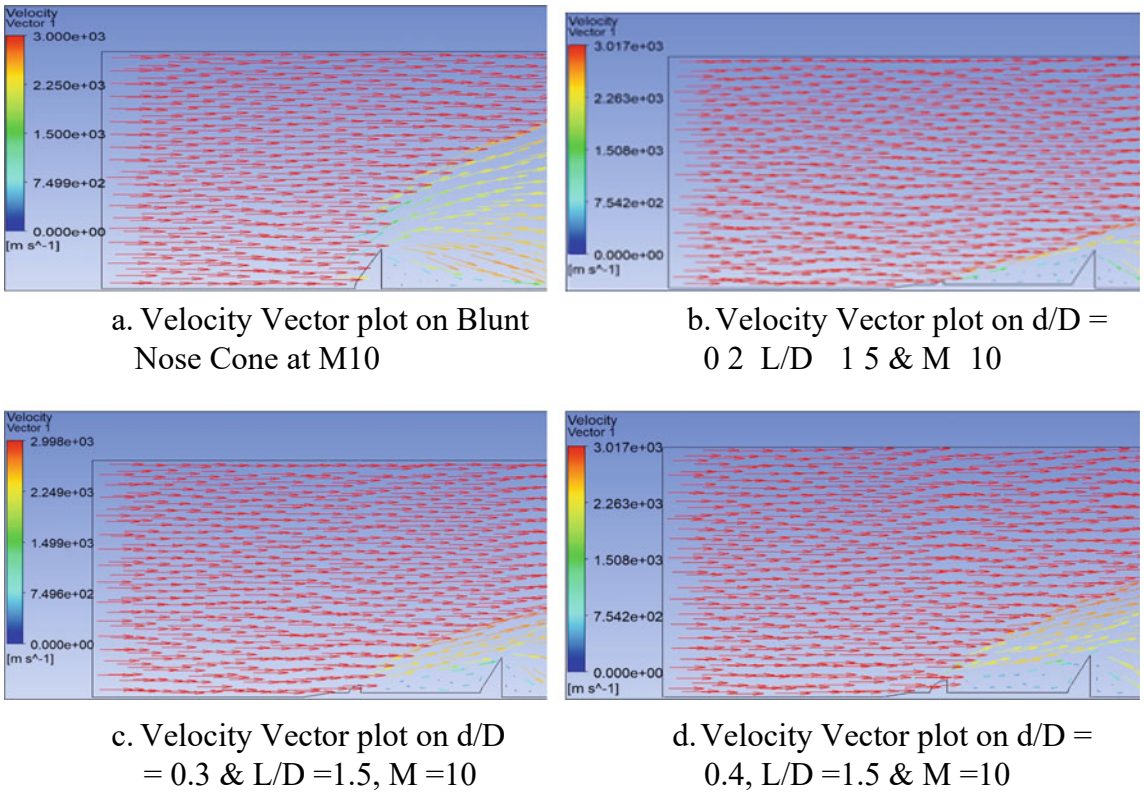

Fig. 12 Velocity Vector distribution over the nose cone with and without aerospike and aerodisk at L/D ratio = 1.5

significant shock pattern takes place at d/D ratios of 0.2, 0.3, and 0.4. The strength of shock formation is slightly higher than other L/D ratios such as 1 and 1.5.

3.2 Velocity Contour of Blunt Nose Cone with and Without Aerospike and Aerodisk at Mach Number 10

The velocity distribution over the blunt cone was investigated for Mach number of 10 represented with velocity contour gives flow physics to analyze the behavior to find shock pattern over the blunt nose cone with and without L/D ratio and d/D ratio as shown in Figs. 8, 9 and 10.

3.2.1 Velocity Contour at Different D/D, L/D = 1 and Mach Number, M = 10

For analysis and for a better understanding of the differences, the evolution of the flow file around the blunt nose cone with and without the aerodisk and aerospike depicted in Fig. 8a–d is compared. The shock pattern is formed away from the blunt nose cone's tip by a minor increase in the velocity contour at Fig. 8a upstream of the cone's blunt tip. The shock pattern is formed in the blunt nose cone with an aerodisk and aerospike, as shown in Fig. 8b–d, and an intersect shock pattern is formed behind the nose cone very far away. At the ratio of L/D = 2, the creation of a very significant shock pattern takes place at d/D ratios of 0.2, 0.3, and 0.4. The strength of shock formation is slightly higher than other L/D ratios such as 1 and 1.5.

3.2.2 Velocity Contour at Different D/D, L/D = 1.5 and Mach Number, M = 10

Figure 9a–d illustrates the investigation of the velocity vector growth around the blunt nose cone with and without the aerodisk and aerospike

The shock pattern is formed away from the blunt nose cone's edge by a slight increase in the velocity contour at Fig. 9a upstream of the cone's blunt edge. The shock pattern is formed in the blunt nose cone with an aerodisk and aerospike, as shown in Fig. 9b–d, and an intersect shock pattern is formed behind the nose cone very far away. At the ratio of L/D = 2, the formation of a significant shock pattern takes place at d/D ratios of 0.2, 0.3, and 0.4.

3.2.3 Velocity Contour at Different D/D, L/D = 2 and Mach Number, M = 10

The evolution of the flow file around the unsharpened and dull conoid of nose with the application as well as without the usage of the aerodisk and aerospike shown in Fig. 8a–d

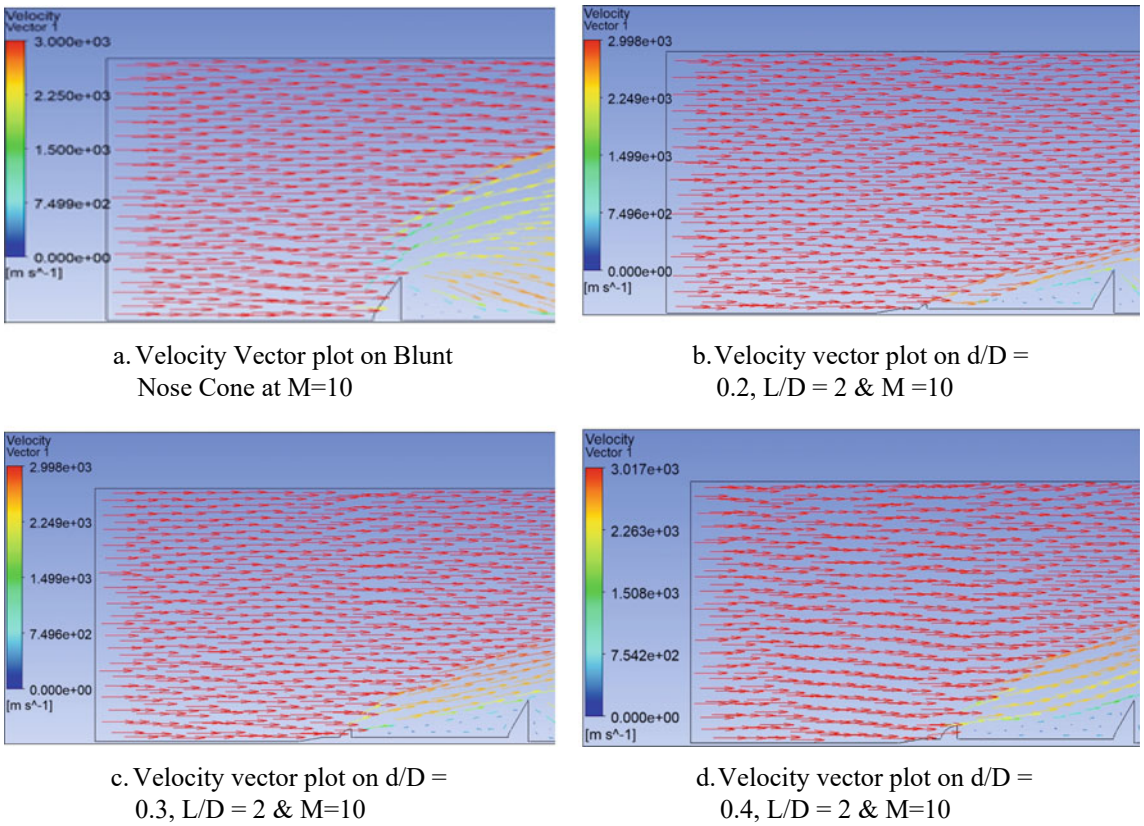

a. Velocity Vector plot on Blunt Nose Cone at M=10

b. Velocity vector plot on d/D = 0.2, L/D = 2 & M =10

c. Velocity vector plot on d/D = 0.3, L/D = 2 & M=10

d. Velocity vector plot on d/D = 0.4, L/D = 2 & M=10

Fig. 13 Velocity vector distribution over the nose cone with and without aerospike and aerodisk at L/D ratio = 2

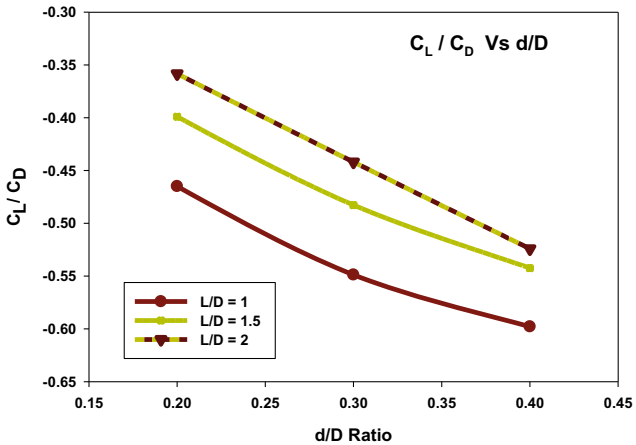

Fig. 14 CL / CD ratio versus d/D ratio

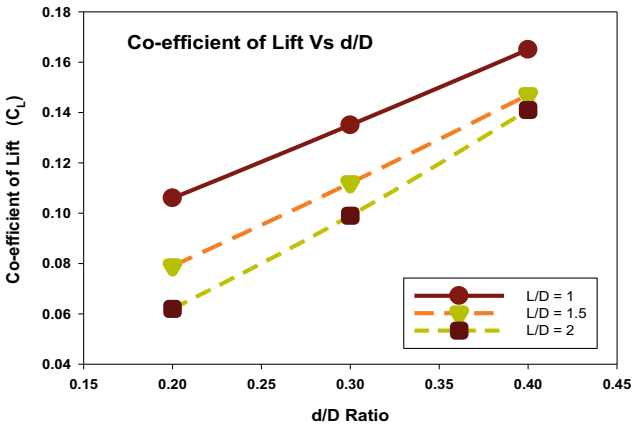

Fig. 15 CL versus d/D ratio

is analyzed to understand the difference. The shock pattern is formed away from the blunt nose cone's tip by a minor increase in the velocity contour at Fig. 8a upstream of the cone's blunt tip. The shock pattern is formed in the blunt nose cone with an aerodisk and aerospike, as shown in Fig. 8b–d, and an intersect shock pattern is formed behind the nose cone very far away. At the ratio of L/D = 2, the creation of a very significant shock pattern takes place at d/D ratios of 0.2, 0.3, and 0.4. The strength of shock formation is slightly higher than other L/D ratios such as 1 and 1.5.

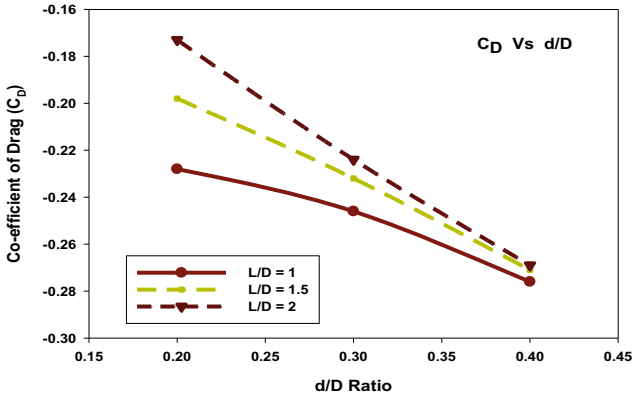

Fig. 16 CD versus d/D ratio

3.3 Velocity Vector Plot of Blunt Nose Cone with and Without Aerospike and Aerodisk at Different Mach Numbers

The distinct difference of flow features as well as velocity vector creations over the blunt nose cone with and without different L/D ratio and d/D ratio with Mach number of 10 is clearly shown in Figs. 11, 12 and 13.

3.3.1 Velocity Vector at Different D/D Ratios, L/D = 1 and Mach Number, M = 10

The streamlined flow over the blunt nose cone described by the velocity vector is shown in Fig. 5a and decelerated flow gets diverted and moves slightly away from the tip of the nose cone. But in the case of a blunt nose cone with aerodisk and aerospike, the flow accelerated behind the aerodisk is very closer to the aerospike by an increase in d/D as shown in Fig. 11b–d.

3.3.2 Velocity Vector at Different D/D, L/D = 1.5 and Mach Number, M = 10

The streamlined flow over the blunt nose cone described by the velocity vector is shown in Fig. 12a and the decelerating flow becomes sidetracked and drifts away from the nose cone's tip. But with a blunt nose cone equipped with an aerodisk and an aerospike, the flow accelerated behind the aerodisk very closer to the aerospike by an increase in d/D as shown in Fig. 12b–d.

3.3.3 Velocity Vector at Different D/D, L/D = 2 and Mach Number, M = 10

The streamlined flow over the blunt nose cone where described by the velocity vector is shown in Fig. 13a and decelerated flow gets diverted and moves slightly away from the tip of the nose cone. But in the case of blunt nose cone with aerodisk and aerospike, the flow accelerated behind the aerodisk very high compared with other d/D [0.2 &0.3] and closer to the aerospike very high d/D as shown in Fig. 13b–d.

3.4 Effect of Lift Co-efficient and Drag Co-efficient on Blunt Nose Cone with and Without Aerodisk and Aerospike with Mach Number of 10

The lift coefficient and drag coefficient play vital roles in the blunt nose cone and the research carried out provides us enough evidence that shows and proves the size of the aerodisk, and aerospike is having a significant impact involved in the decrease of drag. It is explored that aerospike and aerodisk diameter influences the pressure drag and lift during high-speed flow with Mach number 10 and it was clearly represented in Figs. 14 and 16. The coefficient of drag with different geometry of d/D = 02, 0.3 and 0.4 (d/D describes the ratio of aerodisk diameter to blunt nose diameter. It observed that the lift coefficient is not significant but accounted for in our study illustrated in Fig. 15 which shows that the lift coefficient is more effective in L/D = 1 increase with an increase in the aerodisk diameter than other L/D locations. In the case of the drag coefficient in Fig. 14, it is observed that drag reduction was influenced by an increase in aerodisk diameter at L/D = 1.

4 Conclusion

In this paper, the aerodisk assembly's sharp spike is intended to lessen the drag and aerodynamic heating. Mach number 10 free stream testing was conducted on the setup. The spiky aerodisk configuration outperformed two conventional configurations with a maximum drag reduction of 37.73%. The flow field around this arrangement demonstrated that it was better to separate the entering flow than the normal hemispherical aerodisk and the acute spike. As the length of the spike and diameter increases, the percentage of drag reduction increases. The peak heating value and static pressure on the blunt hemisphere surface both significantly dropped as a result of this idea being proposed. From the analysis, the reduction of drag does not work on the higher Mach speed. The shape hemi-spherical is likely more convenient than the blunt body for heat dissipation and drag reduction. In this research work, the results of the current study show that the shock pattern varies significantly closer to the nose cone model at L/D ratio 2 and that variations in drag reduction occur as a result of increasing d/D ratio and aerospike. Also, the flow pattern over the model was thoroughly examined.

References

Balaji, G., Senthil Kumar, C., Nadaraja Pillai, S., & Senthil Kumar, R. (2015). Aerodynamic performance enhancement of blunt body using aero disk. *International Journal of Applied Engineering Research, 10*(33).

Balaji, G., Sree, K. N., Reddy, E. V., Sumanth, N., Sathish, S., & Madhanraj, V. (2022). Numerical investigation of flow over a hemispherical missile nose cone configuration in subsonic speed. *Materials Today: Proceedings, 68*, 1447–1454.

Deng, F., Jiao, Z., Liang, B., Xie, F., & Qin, N. (2017). Spike effects on drag reduction for hypersonic lifting body. *Journal of Spacecraft and Rockets, 54*(6), 1185–1195.

Elsamanoudy, M., Ghorab, A., & Hendy, M. (2013, May 28–30) Drag reduction using spiked-aerodisk & reattachment ring for hypersonic hemispherical bodies. In *International Conference on Aerospace Sciences and Aviation Technology* (Vol. 15). Aerospace Sciences & Aviation Technology, ASAT-15 (pp. 1–16). The Military Technical College.

Hamid, A. H. A., Salleh, Z., Suloh, A. M. I. M., Sujana, M. J., Saad, M. S., & Khamis, M. I. (2022). Evaluation of a newly designed aerodisk for cloud seeding prototype rocket drag reduction. *Pertanika Journal of Science & Technology, 30*(2)

Kalimuthu, R., Mehta, R. C., & Rathakrishnan, E. (2008). Experimental investigation on spiked body in hypersonic flow. *The Aeronautical Journal, 112*(1136), 593–598.

Schnepf, Ch., Wysocki, O., & Schülein, E. (2015). Wave drag reduction due to a self-aligning aerodisk. *Progress in Flight Physics, 7*, 475–488.

Senthilkumar, S., Mudholkar, A. A., & Sanjay, K. J. (2021). A comparative study on aerodynamic drag reduction of a blunt nose body using aerospike and aerodisk–numerical approach. In *IOP Conference Series: Materials Science and Engineering, 1130*(1), 012074. IOP Publishing.

Wysocki, O., Schülein, E., & Schnepf C. (2014). Experimental study on wave drag reduction at slender bodies by a self-aligning aerospike. In *New Results in Numerical and Experimental Fluid Mechanics* (Vol. IX, pp. 583–590). Cham: Springer.